Appendix A. Supplementary Material

A Cerebral Cortex-like Structured Metallized Elastomer for High-Performance Triboelectric Nanogenerator

Moon Kyu Park[a], Seokmin Lee[a], Yongmin Ko[b] and Jinhan Cho[a,c,d]*

[a]Department of Chemical & Biological Engineering, Korea University, 145 Anam-ro, Seongbuk-gu, Seoul 02841, Republic of Korea

[b]Division of Energy Technology, Daegu Gyeongbuk Institute of Science and Technology (DGIST), 333 Techno Jungang-daero, Hyeonpung-eup, Dalseong-gun, Daegu 42988, Republic of Korea

[c]KU-KIST Graduate School of Converging Science and Technology, Korea University, 145 Anam-ro, Seongbuk-gu, Seoul 02841, Republic of Korea

[d]Soft Hybrid Materials Research Center, Advanced Materials Research Division, Korea Institute of Science and Technology (KIST), 5 Hwarang-ro 14-gil, Seongbuk-gu, Seoul 02792, Republic of Korea

*Corresponding author.

E-mail addresses: jinhan71@korea.ac.kr (J. Cho)

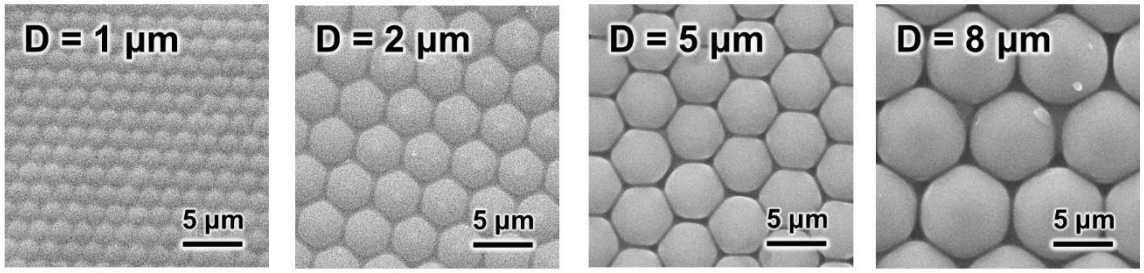

Figure S1. Embossed PDMS with diameters of 1 µm, 2 µm, 5 µm and 8 µm.

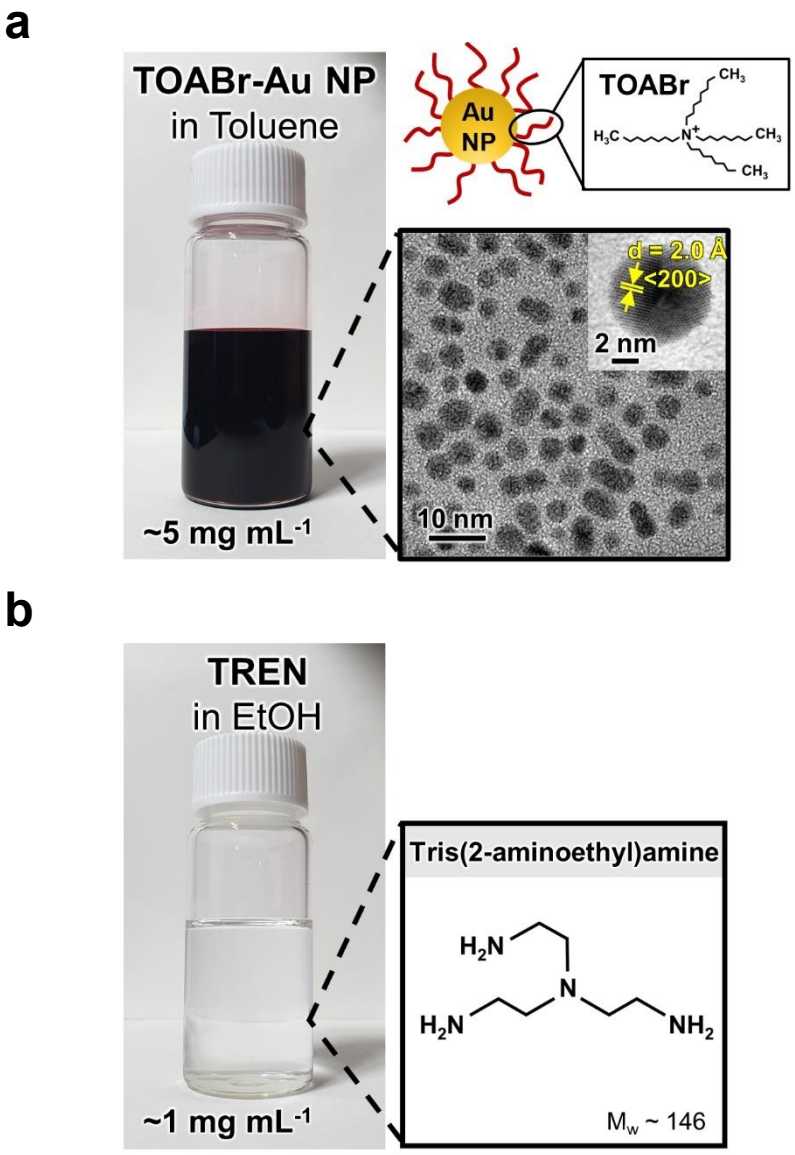

Figure S2. (a) Digital image of TOABr-Au NP dispersed in toluene. Expanded image shows the TEM image of TOABr-Au NPs with diameters of roughly 7 nm, while the inset shows a lattice spacing of about 2.0 Å. Schematic diagram shows an illustration of Au NP surrounded by TOABr ligands, while the expanded image shows the chemical structure of TOABr. (b) Digital image of TREN disperse in EtOH. Expanded image shows the chemical structure of TREN.

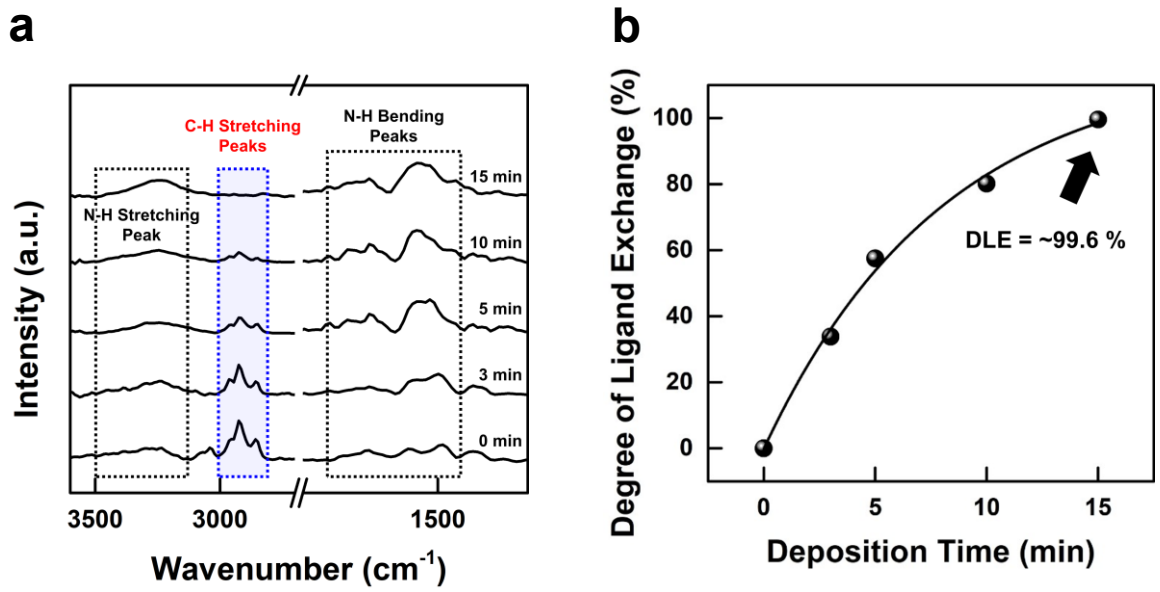

Figure S3. (a) FTIR spectra of (TOABr-Au NP/TREN)$_2$-deposited Si wafer at different final TREN deposition time. In this case, the intensity of C-H stretching peaks decreases as deposition time of TREN increases, resulting in complete ligand exchange at 15 min. (b) Degree of ligand exchange (DLE) occurring during TREN deposition time was calculated through the intensity area change of the C-H stretching peaks. At deposition time of 15 min, the remaining TOABr ligands was estimated to be approximately 0.4 % (DLE of 99.6%).

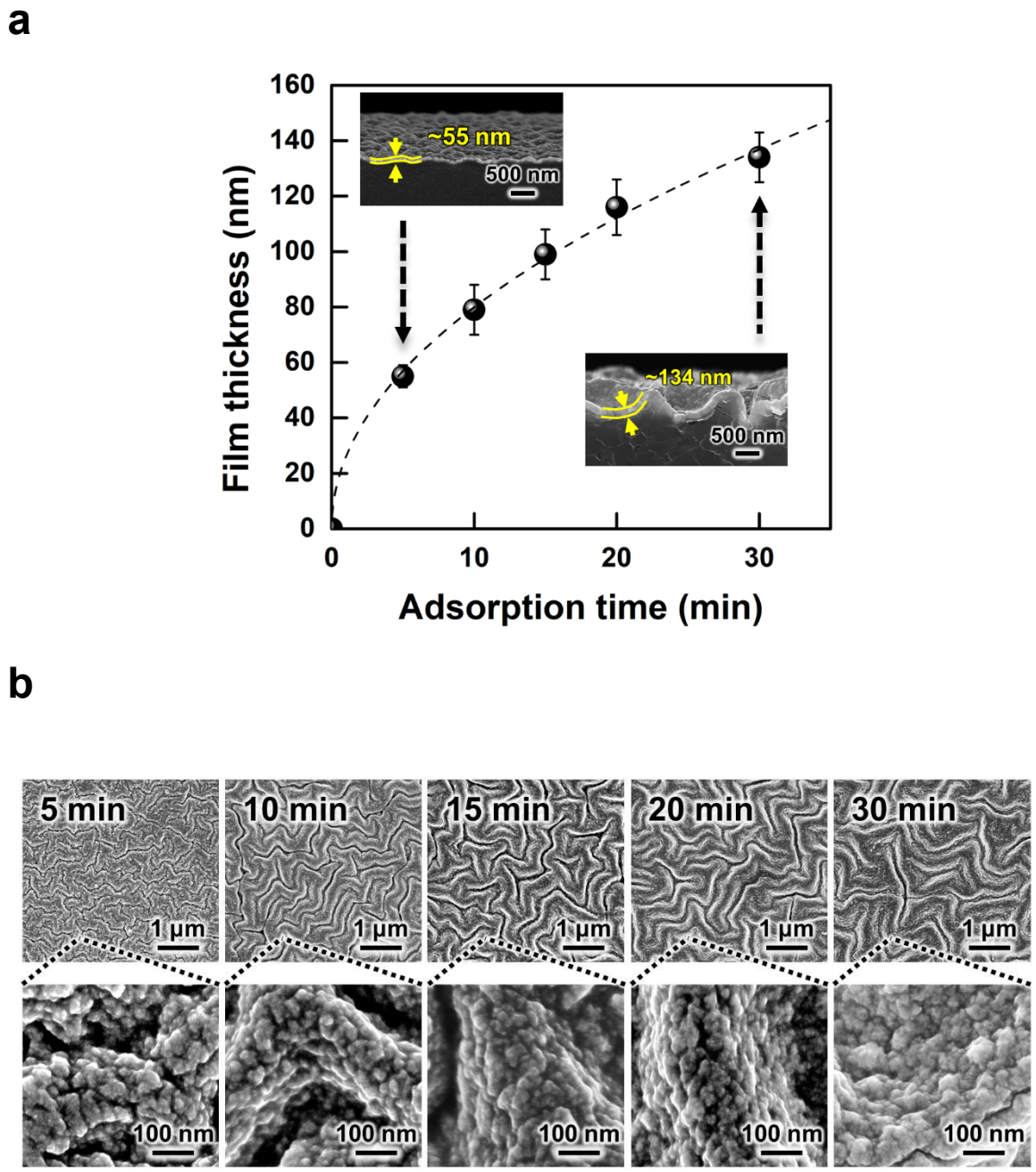

Figure S4. (a) Film thickness data with cross-sectional FE-SEM images (inset) and (b) planar FE-SEM images of TOABr-Au NP-assembled flat SH-PDMS with increasing adsorption time from 1 minute to 30 minutes.

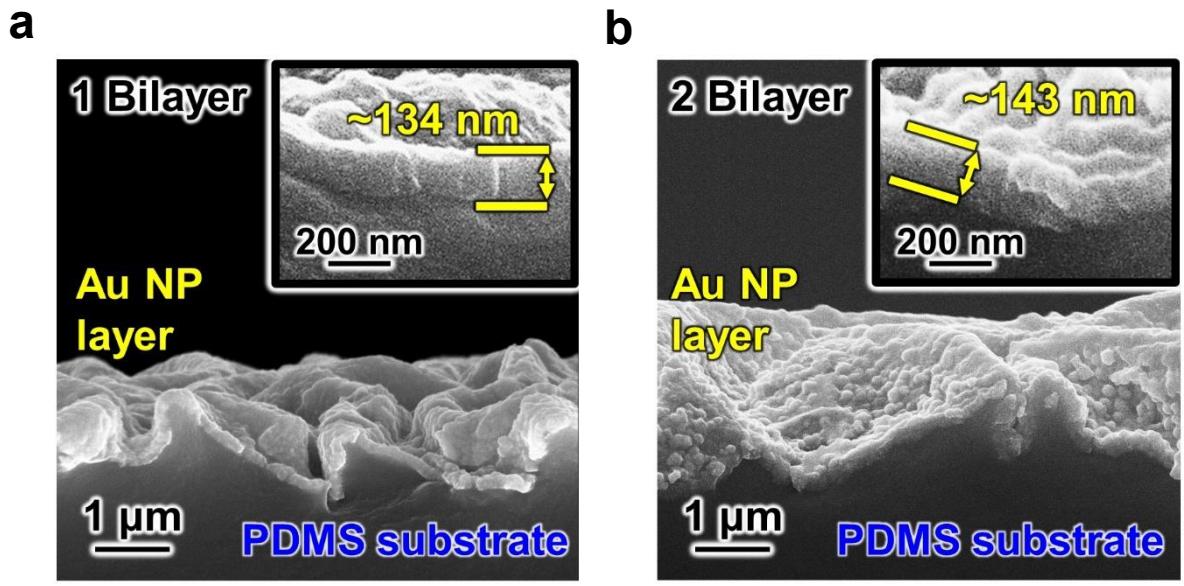

Figure S5. (a) Cross-sectional FE-SEM image of $(TOABr\text{-}Au\ NP/TREN)_1$ and (b) $(TOABr\text{-}Au\ NP/TREN)_2$, showing the thickness change of the Au NP layer.

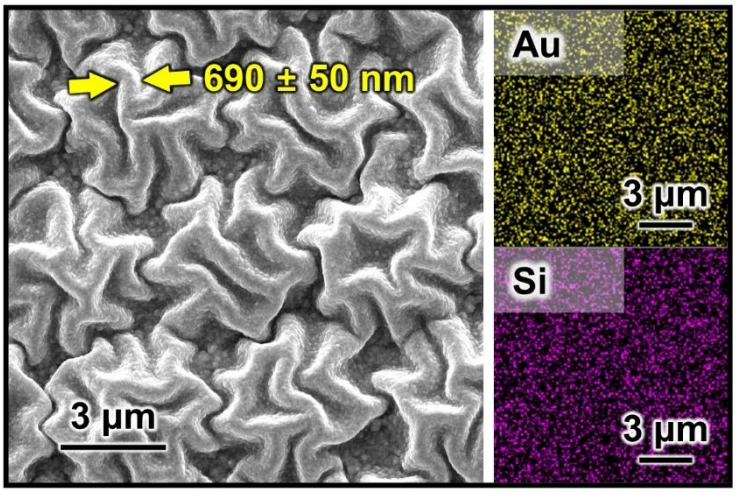

Figure S6. FE-SEM image and energy-dispersive X-ray spectroscopy (EDS) mapping image of $(TOABr\text{-}Au\ NP/TREN)_1$-PDMS film.

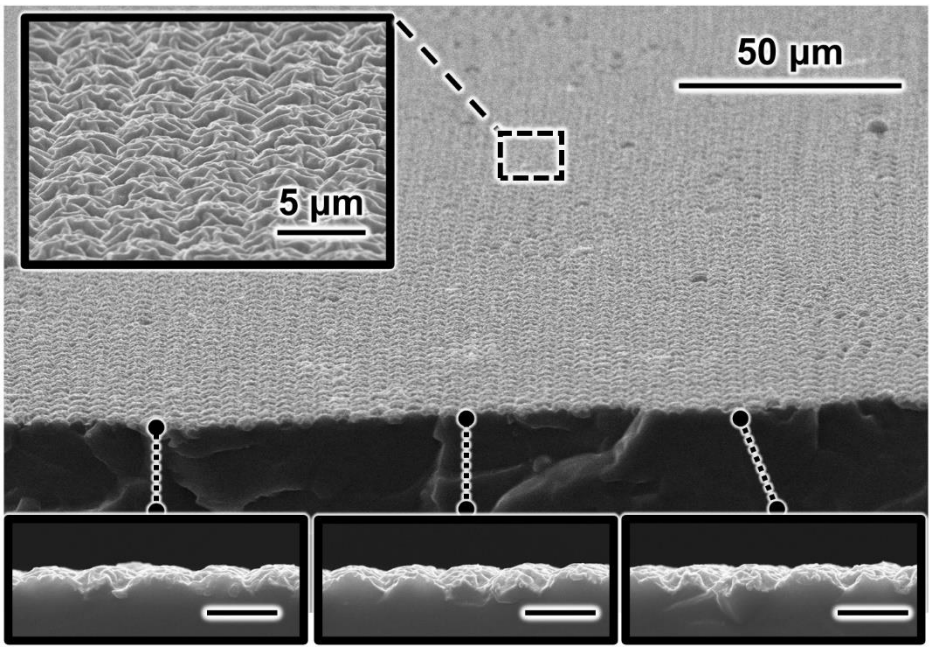

Figure S7. Low resolution tilted SEM image of $(TOABr\text{-}Au\ NP/TREN)_1$-deposited embossed PDMS showing the isotropic and very uniformly formed wrinkles throughout the sample. Top inset shows a magnified SEM image of the sample surface. Bottom insets show the cross-sectional SEM images of $(TOABr\text{-}Au\ NP/TREN)_1$ bilayer seamlessly coated on top of the PDMS substrate, without indication of delamination. The scale bars at the bottom insets represent 5 μm in length.

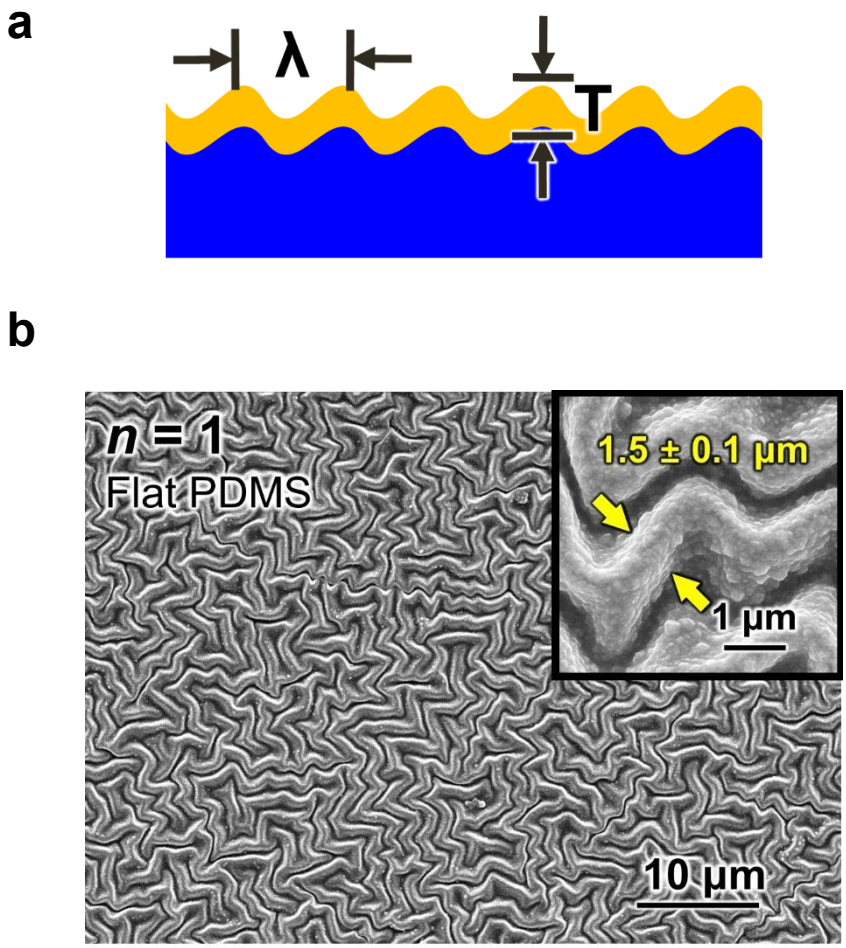

Figure S8. (a) Schematic illustration of the cross-sectional composition of (TOABr-Au NP/TREN)$_1$-deposited flat PDMS. The golden layer represents a single bilayer of (TOABr-Au NP/TREN), while the blue component represents the PDMS substrate. Here, λ and T represents the wavelength of the wrinkle pattern and thickness of (TOABr-Au NP/TREN)$_1$ bilayer, respectively. (b) FE-SEM image of (TOABr-Au NP/TREN)$_1$-deposited flat PDMS.

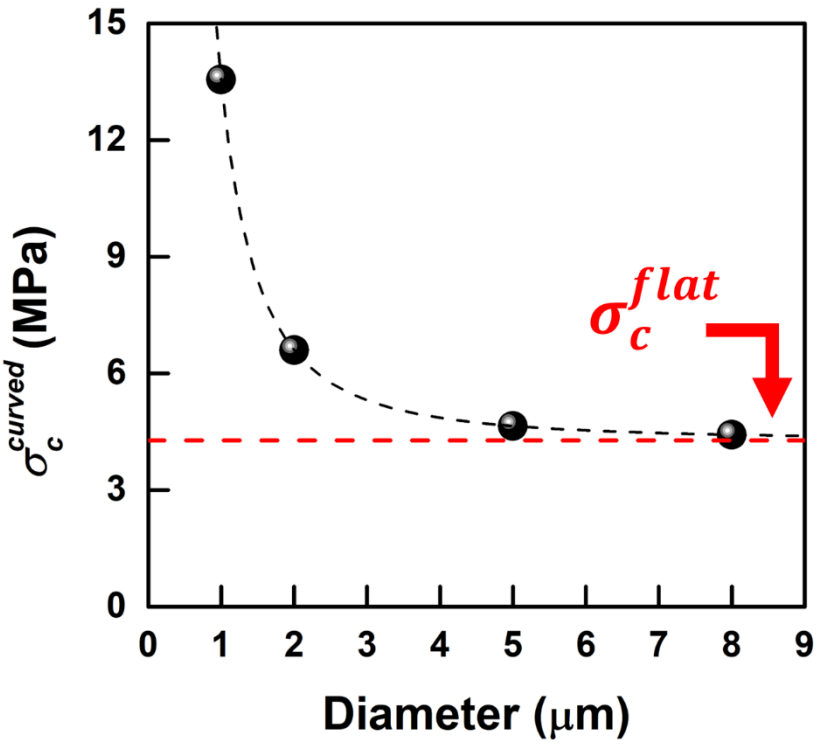

Figure S9. Critical stress of $(TOABr\text{-}Au\ NP/TREN)_1$-coated embossed PDMS with different diameters based on Equation 3. The parameters used are T = 134 nm, E_s = 2.4 MPa, E_f = 5.4 MPa, and ν_s = 0.5. The red line indicates the value for σ_c^{flat}.

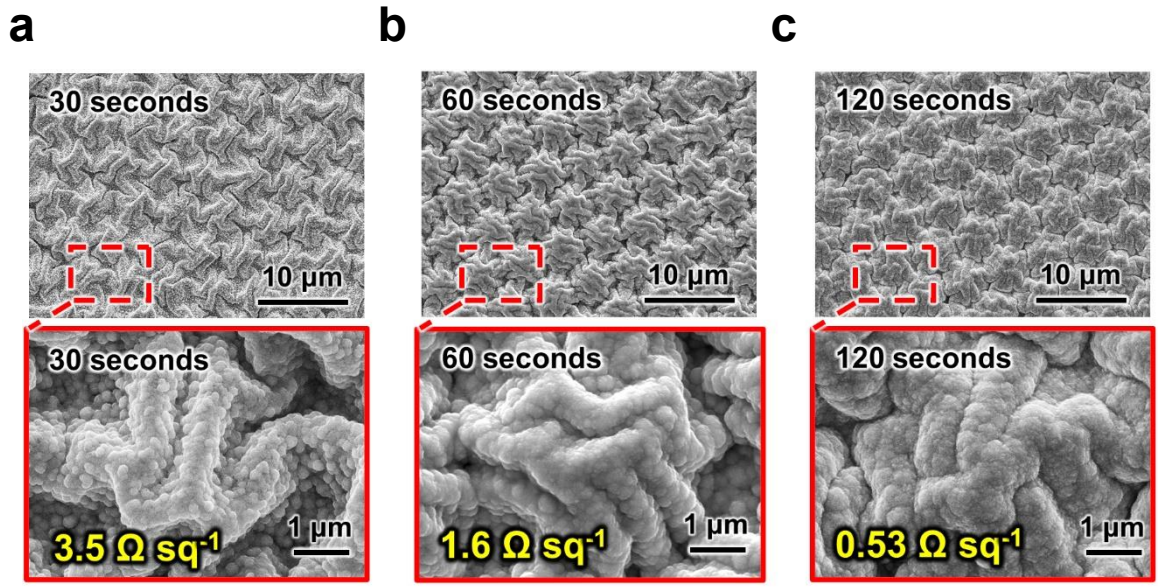

Figure S10. FE-SEM images of the (TOABr-Au NP/TREN)$_2$-coated embossed PDMS after (a) 30 seconds, (b) 60 seconds, and (c) 120 seconds of Ni electroplating at 25 mA cm^{-2}.

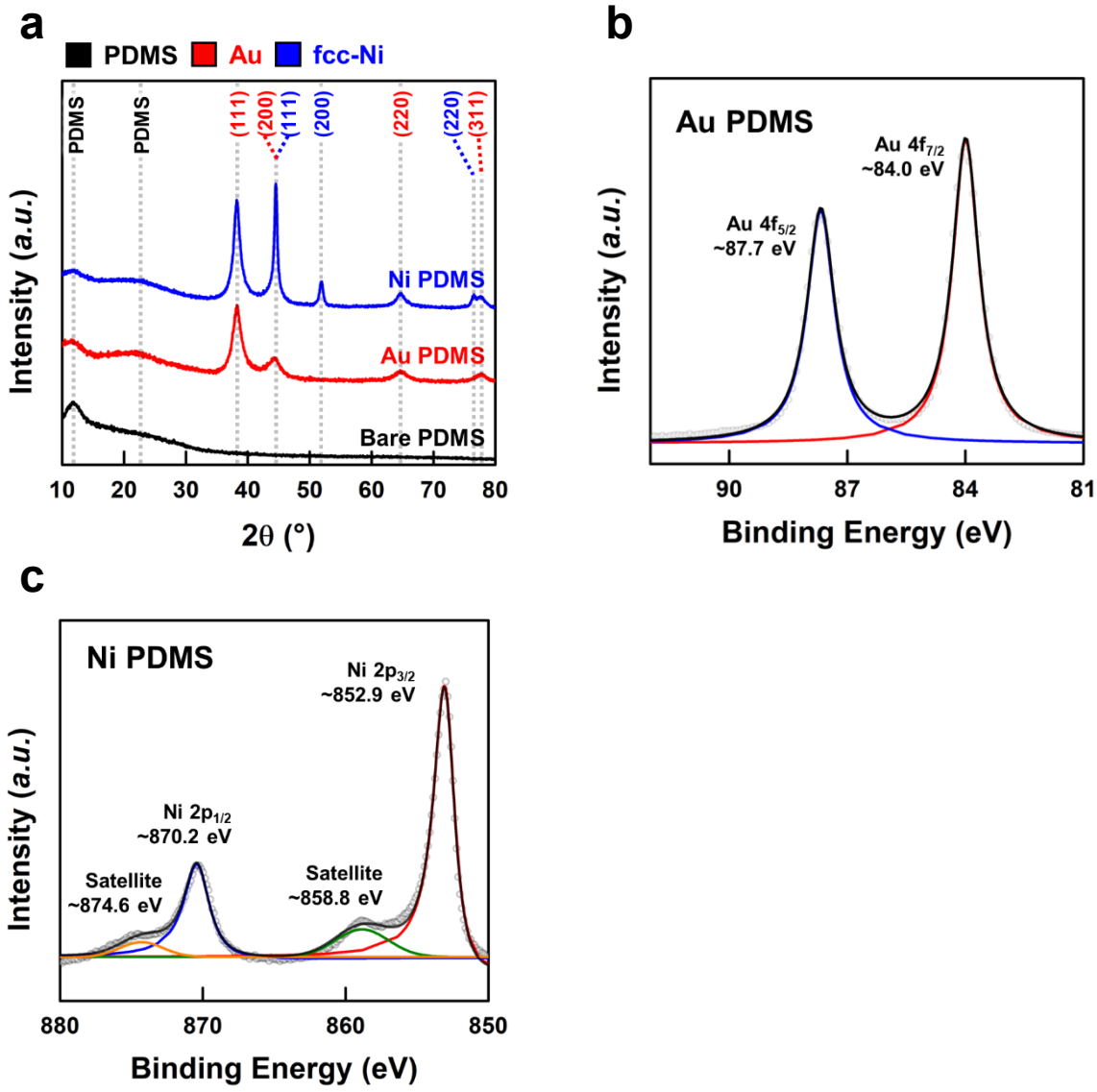

Figure S11. (a) XRD analysis of Au NP-coated and Ni-electroplated PDMS electrode's crystal structure. For Ni PDMS, reflection peaks were detected at 44.6°, 52.0° and 76.5°, which corresponds to (111), (200) and (220) planes of fcc-Ni. The JCPDS file numbers of Au and fcc-Ni are 04-0784 and 04-0850, respectively. (b) XPS analysis of the Au NP-coated PDMS electrode's surface states. (c) XPS analysis of the Ni-electroplated PDMS electrode's surface states. Peaks were seen at binding energies 870.2 and 852.9 eV, corresponding to Ni $2p_{1/2}$ and Ni $2p_{3/2}$ respectively, with their satellite peaks at 874.6 eV and 858.8 eV, indicating fcc-Ni structure.

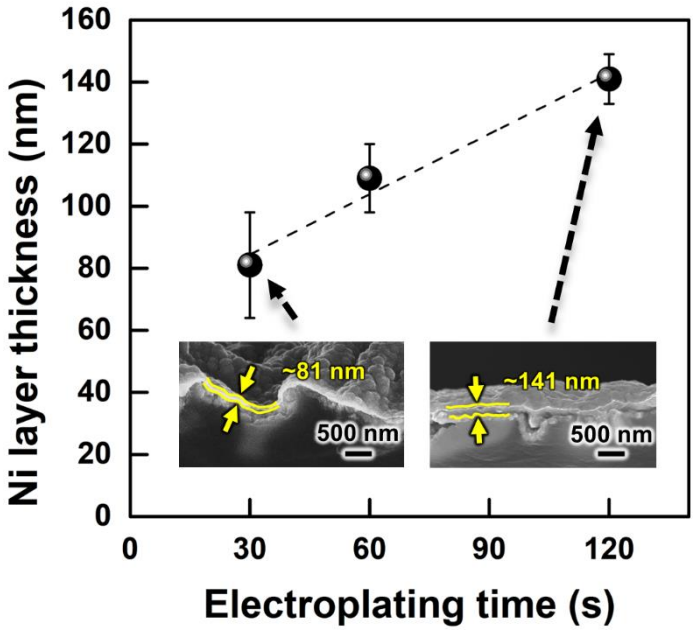

Figure S12. Ni layer thickness data and FE-SEM images (inset) of Ni electroplated PDMS electrode as a function of electroplating time (current density of 25 mA cm^{-2}).

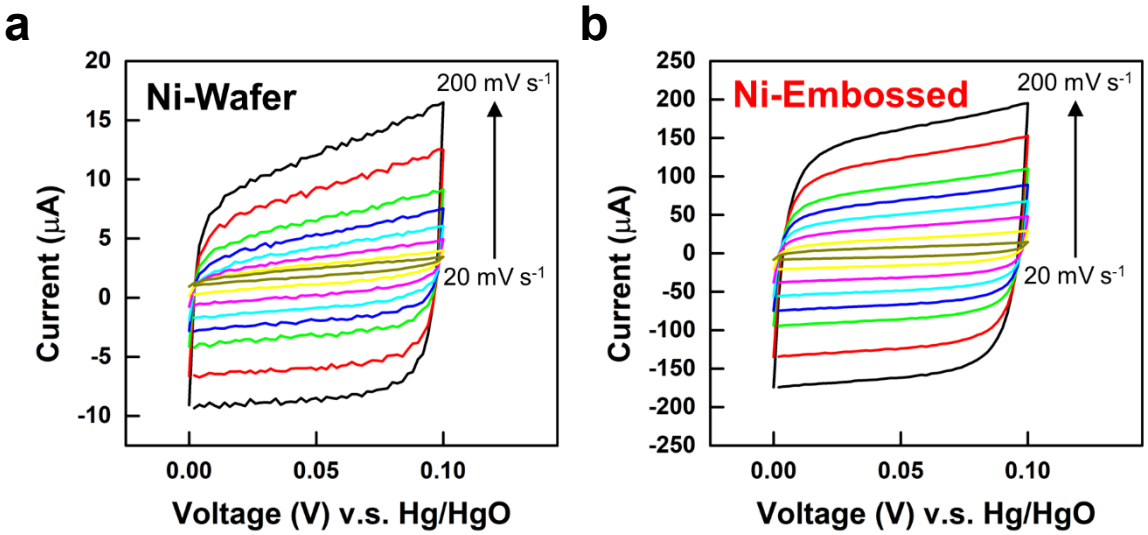

Figure S13. CV curves of (a) Ni-Wafer and (b) Ni-Embossed electrodes in the non-Faradic potential region between 0 to 0.1 V at different scan rates ranging from 20 mV s^{-1} and 200 mV s^{-1}.

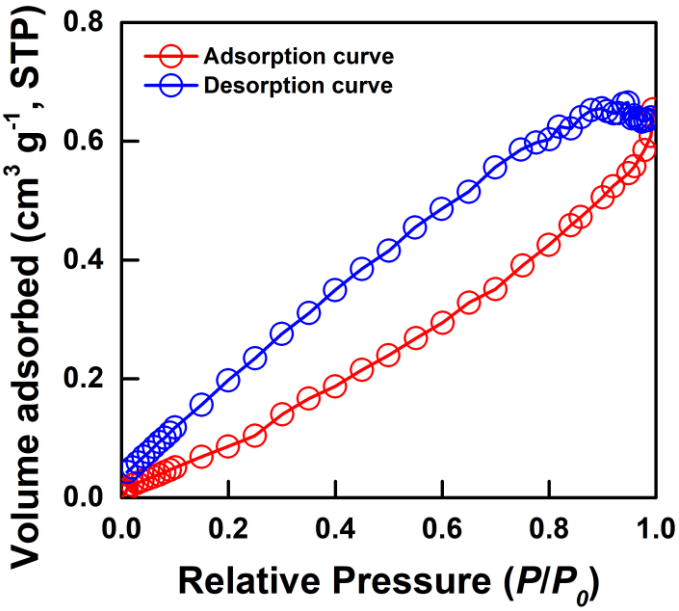

Figure S14. BET analysis of Ni-Embossed electrode. The specific surface area of Ni-Embossed electrode was measured to be ~0.52 m^2 g^{-1}.

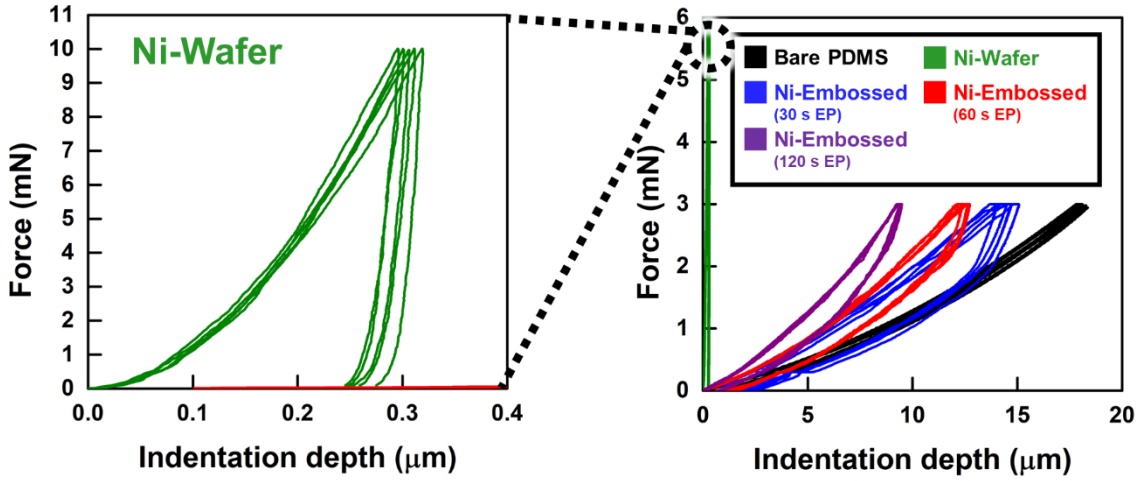

Figure S15. Force displacement graph based on nanoindentation test of bare PDMS, Ni-Wafer, and Ni-Embossed electrodes at various electroplating time. In contrast to PDMS-based electrodes, the maximum indentation depth of Ni-Wafer reached only ~0.3 μm at a force of 12 mN, indicating minimal compressibility.

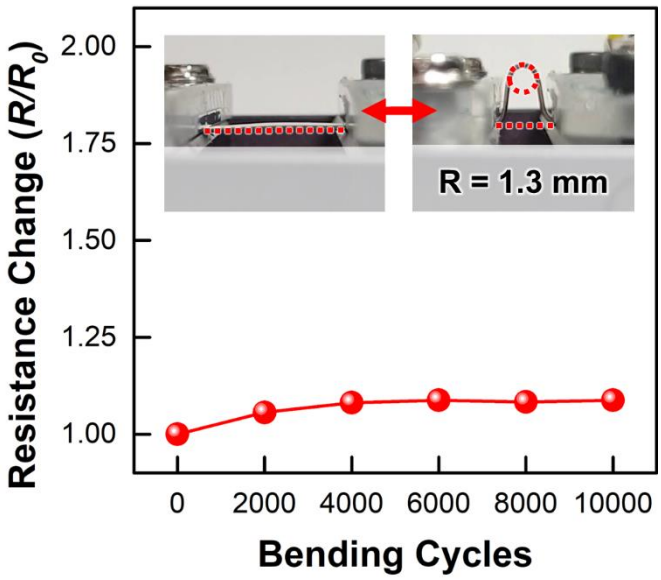

Figure S16. Resistance change (R/R_0) of Ni-Embossed electrode during 10,000 bending cycles under a bending radius of 1.3 mm.

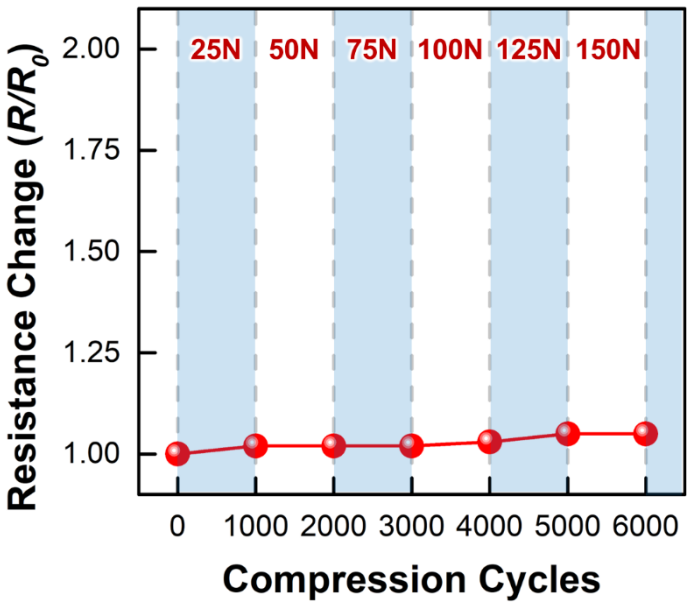

Figure S17. Resistance change (R/R_0) of Ni-Embossed electrode at compressive forces ranging from 25 N to 150N. Compression was repeated for over 1,000 cycles at each force at a frequency of 5 Hz.

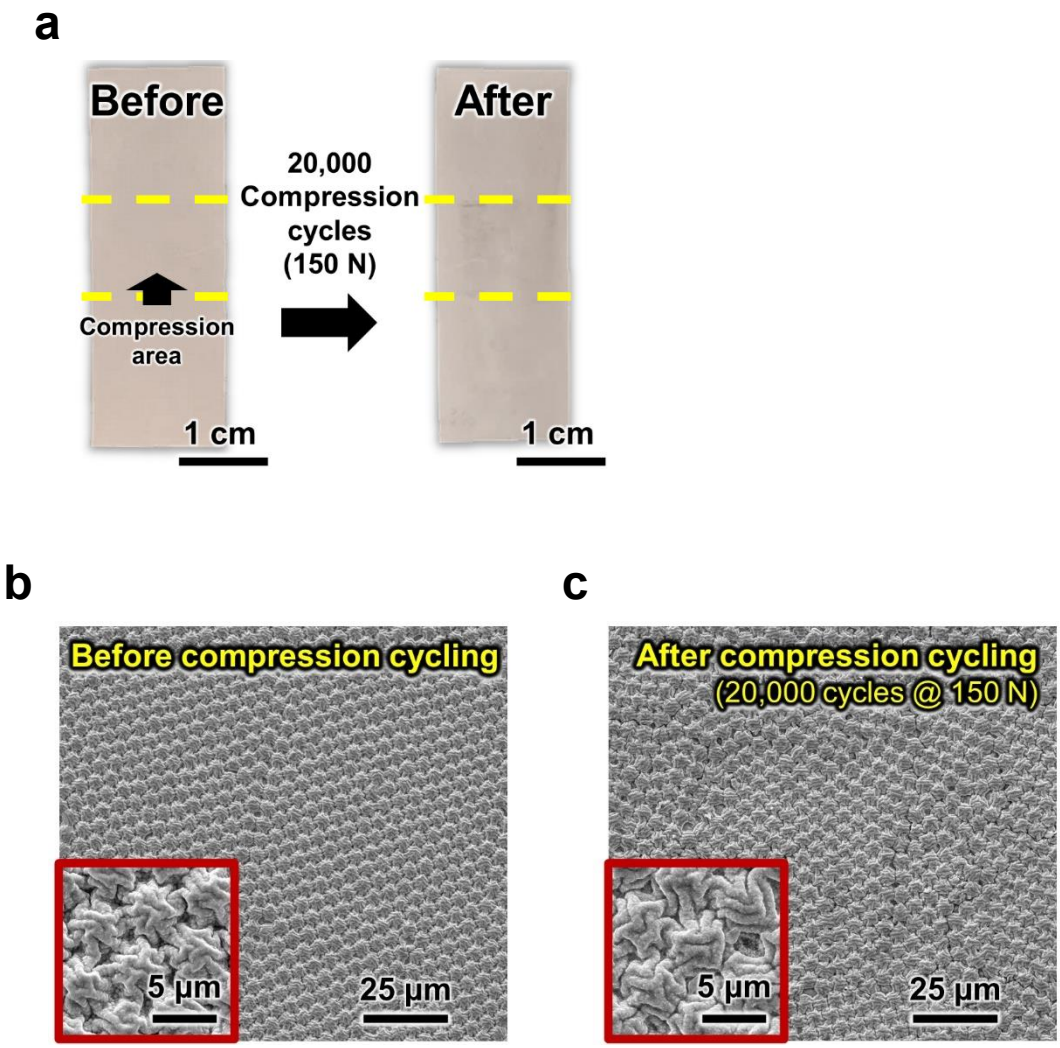

Figure S18. (a) Digital image of Ni-Embossed electrode before and after 20,000 compression cycles at a force of 150 N. Area indicated by the yellow dotted line indicates contact area. FE-SEM images of the compressed region (b) before and (c) after 20,000 compression cycles.

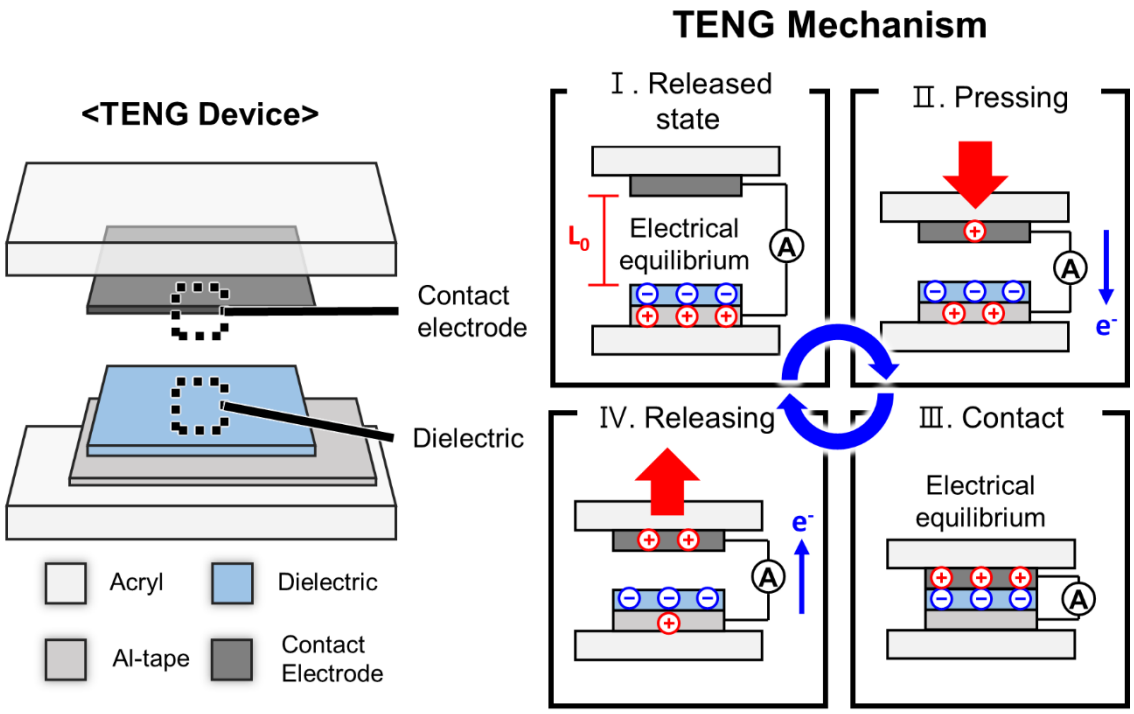

Figure S19. Schematic representation of the TENG device components and the current generation mechanism of TENG. At the released state (I), electrical equilibrium is maintained. (II) Under compressive force, separation length decreases, increasing the electric field strength and therefore creating current across the external circuit. (III) Under contact, the electrode maintains electrical equilibrium. (IV) When the TENG is released, the separation length increases, reducing the electric field strength and therefore creating an opposite current across the external circuit.

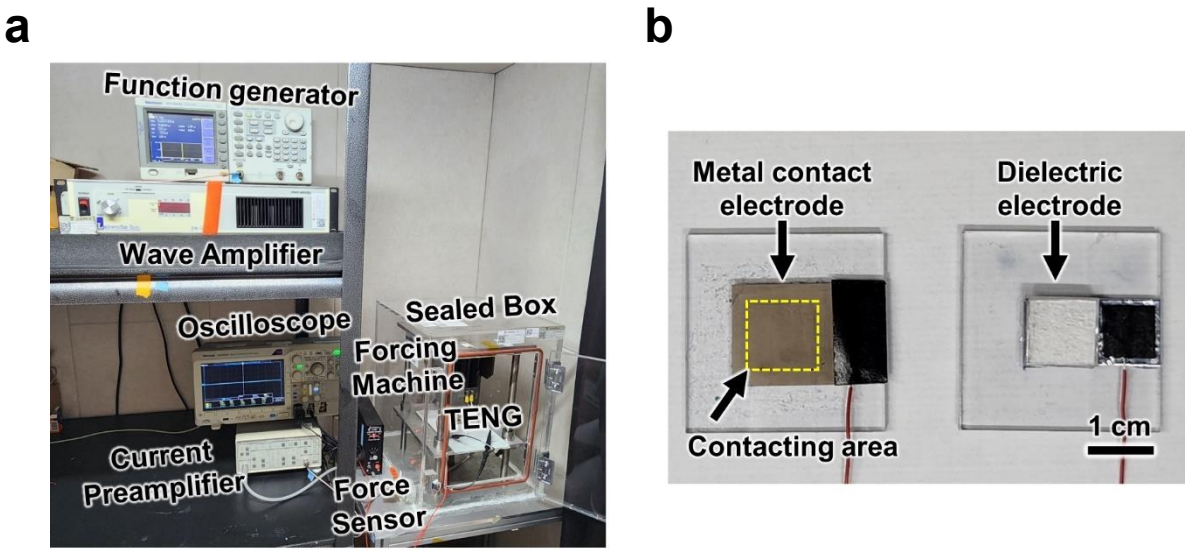

Figure S20. (a) Digital image of the triboelectric performance measuring apparatus. (b) Digital image of the TENG device in its disassembled state. Here, the TENG is composed of Ni-Embossed-based contact electrode and FOTS-Intaglio PDMS dielectric electrode. Copper wire is attached to the metal contact electrode and aluminum tape using conductive tape.

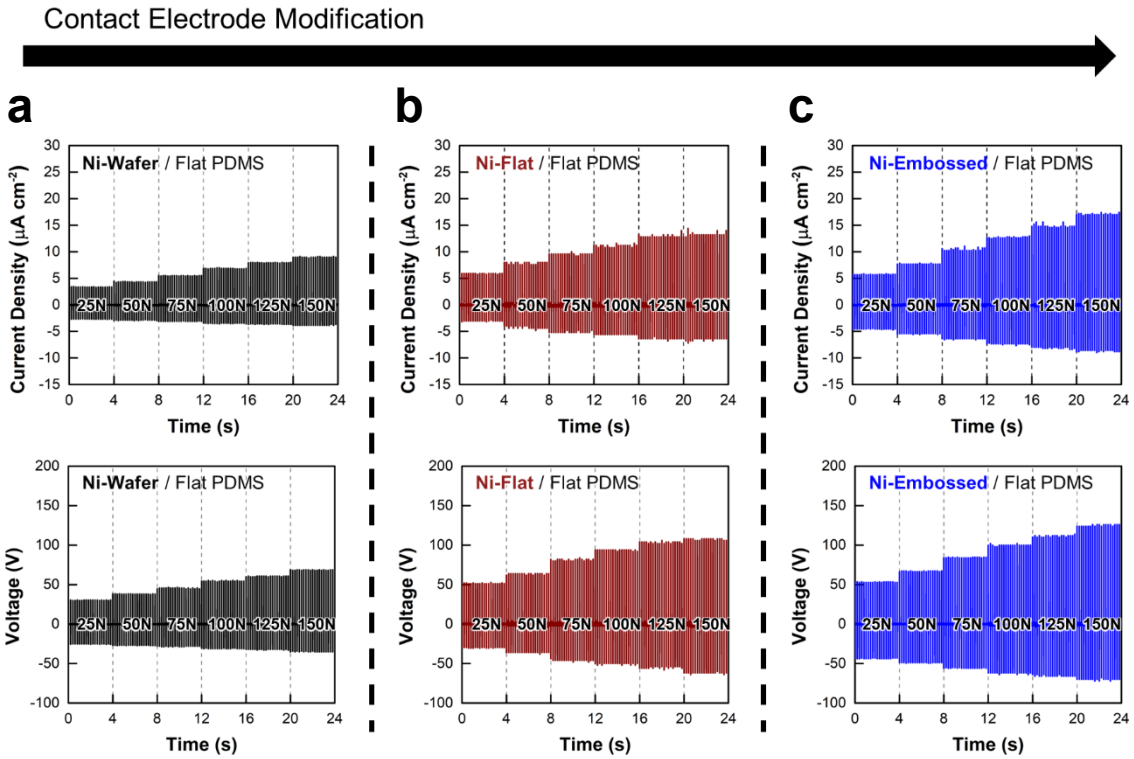

Figure S21. Current density and voltage performance of (a) Ni-Wafer, (b) Ni-Flat and (c) Ni-Embossed electrodes at different forces ranging from 25 N to 150 N. The dielectric electrode used is 1 cm × 1 cm flat PDMS film with a thickness of 500 μm.

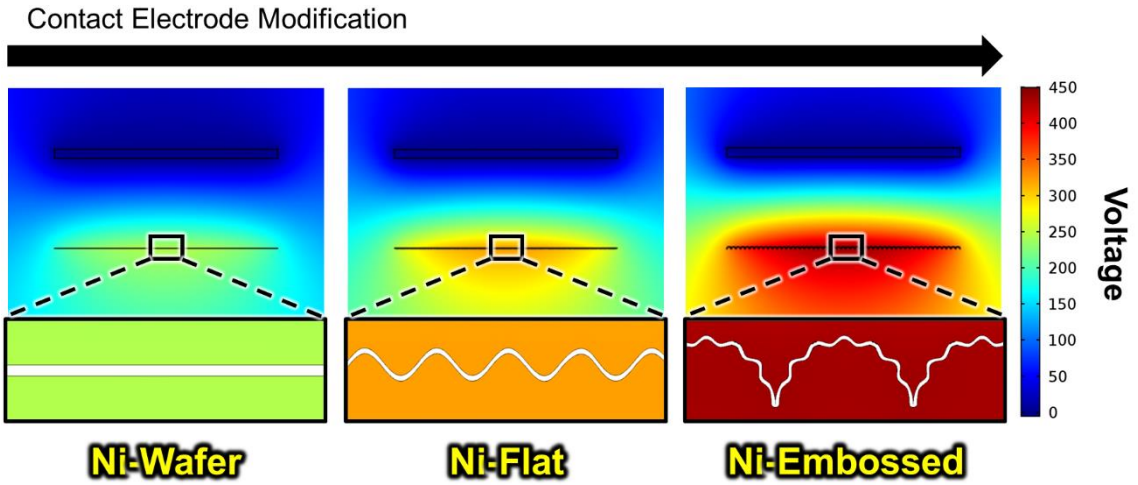

Figure S22. Potential distribution of Ni-Wafer, Ni-Flat and Ni-Embossed electrodes simulated using COMSOL Multiphysics software. During simulation, the electrode distance was fixed at 100 µm. The flat PDMS dielectric electrode dimensions were defined as 250 µm by 10 µm. Ni-Flat electrode wavelength was modelled as a sinusoidal curve of wavelength 1.5 µm, while Ni-Embossed electrode was simulated using a feature size of 5 µm in diameter and 690 nm in wrinkle wavelength. Triboelectric charge density was fixed at 30 µC m^{-2}. The Ni-Embossed electrode is seen to have a greatly increased triboelectric potential compared to Ni-Wafer and Ni-Flat against a flat PDMS dielectric electrode, indicating a greater amount of charge generation with increasing contact.

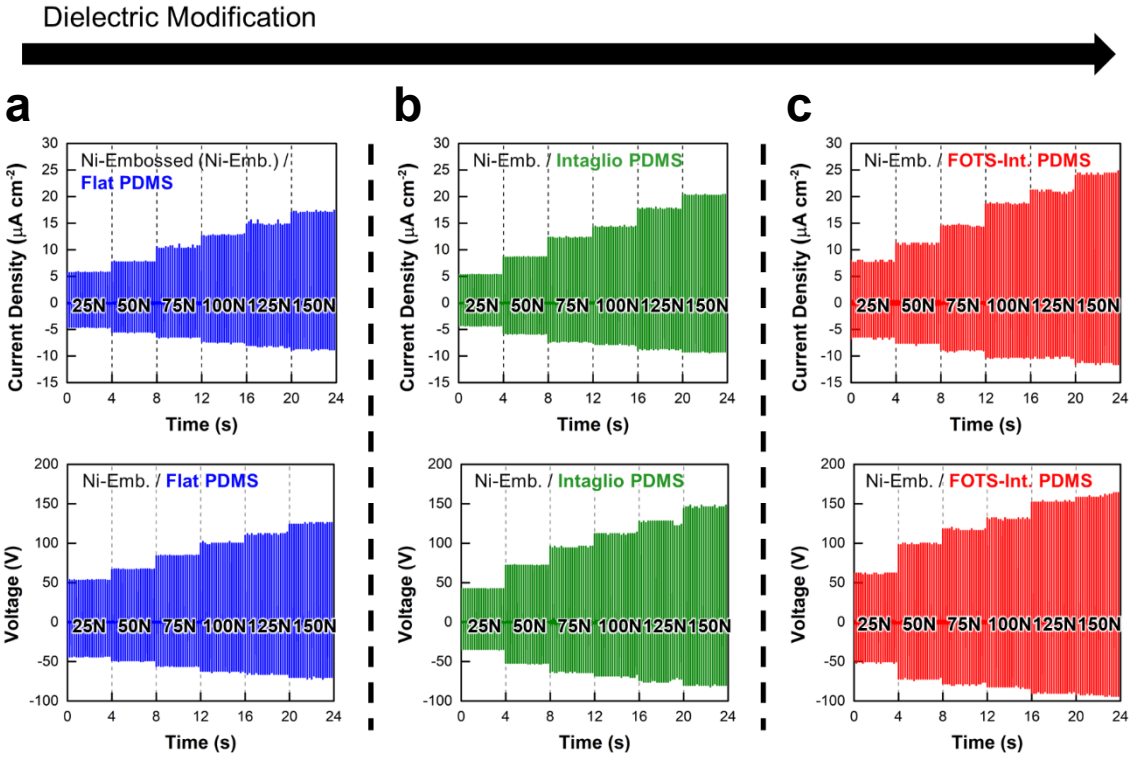

Figure S23. Current density and voltage performance of Ni-Embossed electrode against (a) flat, (b) intaglio and (c) FOTS-intaglio PDMS film dielectric electrodes at different forces ranging from 25 N to 150 N. The dielectric electrode used is 1 cm × 1 cm in dimension with a thickness of 500 μm.

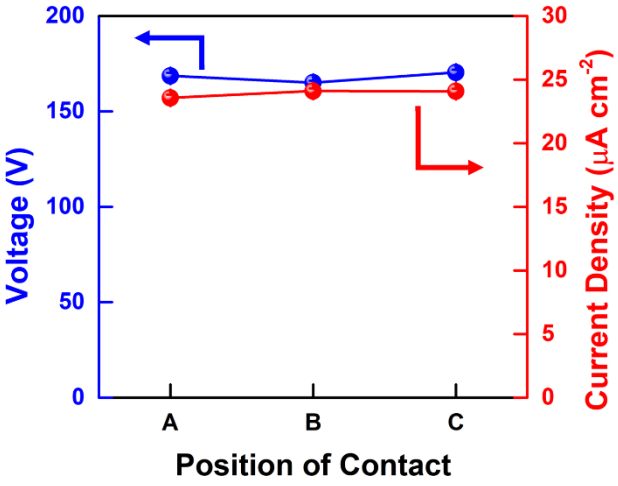

Figure S24. (a) Current density and (b) open circuit voltage response of Ni-Embossed/FOTS-Intaglio PDMS-TENG with Ni-Embossed electrode at different positions of contact with respect to FOTS Intaglio PDMS.